




Article

# Photon Spheres, ISCOs, and OSCOs: Astrophysical Observables for Regular Black Holes with Asymptotically Minkowski Cores

Thomas Berry <sup>\*,†</sup>  Alex Simpson <sup>†</sup>  and Matt Visser <sup>†</sup> 

School of Mathematics and Statistics, Victoria University of Wellington, P.O. Box 600, Wellington 6140, New Zealand; alex.simpson@sms.vuw.ac.nz (A.S.); matt.visser@sms.vuw.ac.nz (M.V.)

\* Correspondence: thomas.berry@sms.vuw.ac.nz

† These authors contributed equally to this work.

**Abstract:** Classical black holes contain a singularity at their core. This has prompted various researchers to propose a multitude of modified spacetimes that mimic the physically observable characteristics of classical black holes as best as possible, but that crucially do not contain singularities at their cores. Due to recent advances in near-horizon astronomy, the ability to observationally distinguish between a classical black hole and a potential black hole mimicker is becoming increasingly feasible. Herein, we calculate some physically observable quantities for a recently proposed regular black hole with an asymptotically Minkowski core—the radius of the photon sphere and the extremal stable timelike circular orbit (ESCO). The manner in which the photon sphere and ESCO relate to the presence (or absence) of horizons is much more complex than for the Schwarzschild black hole. We find situations in which photon spheres can approach arbitrarily close to (near extremal) horizons, situations in which some photon spheres become stable, and situations in which the locations of both photon spheres and ESCOs become multi-valued, with both ISCOs (innermost stable circular orbits) and OSCOs (outermost stable circular orbits). This provides an extremely rich phenomenology of potential astrophysical interest.

**Keywords:** regular black hole; Minkowski core; Lambert W function; black hole mimic.



**Citation:** Berry, T.; Simpson, A.; Visser, M. Photon Spheres, ISCOs, and OSCOs: Astrophysical Observables for Regular Black Holes with Asymptotically Minkowski Cores. *Universe* **2021**, *7*, 2. <https://dx.doi.org/10.3390/universe7010002>

Received: 17 November 2020

Accepted: 17 December 2020

Published: 22 December 2020

**Publisher's Note:** MDPI stays neutral with regard to jurisdictional claims in published maps and institutional affiliations.



**Copyright:** © 2020 by the authors. Licensee MDPI, Basel, Switzerland. This article is an open access article distributed under the terms and conditions of the Creative Commons Attribution (CC BY) license (<https://creativecommons.org/licenses/by/4.0/>).

## 1. Introduction

Karl Schwarzschild first derived the spacetime metric for the region exterior to a static, spherically symmetric source in 1916 [1]; only some 50 years later was it properly understood that this spacetime could be extrapolated inwards to describe a black hole. Without any loss of generality, any static spherically symmetric spacetime can be described by a metric of the form

$$ds^2 = -e^{-2\Phi(r)} \left( 1 - \frac{2m(r)}{r} \right) dt^2 + \frac{dr^2}{1 - \frac{2m(r)}{r}} + r^2 (d\theta^2 + \sin^2\theta d\phi^2). \quad (1)$$

For the standard Schwarzschild metric, one sets  $\Phi(r) = 0$  and  $m(r) = m_0$ . Over the past century, a vast host of black hole spacetimes, qualitatively distinct from that of Schwarzschild, have been investigated by multiple researchers [2–14].

Furthermore, the field has now grown to not only include classical black holes, but also quantum-modified black holes [15–18], regular black holes [19–23], and various other exotic spherically symmetric spacetimes that are fundamentally different from black holes but mimic many of their observable phenomena (e.g., traversable wormholes [24–39], gravastars [40–46], ultracompact objects [47,48], etc. [49–51]; see [52] for an in-depth discussion). Herein, we investigate a specific model spacetime representing a regular black hole. That is, a spacetime that has a well-defined horizon structure, but the curvature invariants are everywhere finite.

Investigating black hole mimickers is becoming increasingly relevant due to recent advances in both observational and gravitational wave astronomy. Projects such as the Event Horizon Telescope [53–58], LIGO [59,60], and the planned LISA [61] are and will be continuously probing closer to the horizons of compact massive objects (CMOs), and so there is hope that such projects will eventually be able to distinguish between the near-horizon physics of classical black holes and possible astrophysical mimickers [52]. Herein, we focus on photon rings, ISCOs and OSCOs. Modifications to photon rings would potentially affect the images gathered by the EHT. Modifications to ISCOs would potentially affect both accretion disks and the final inspiral and plunge events detected by LIGO. In contrast, OSCOs (outermost stable circular orbits) do not exist for Schwarzschild or Kerr black holes—so *any* evidence for the existence of an OSCO would be of immediate astrophysical interest.

The model spacetime investigated in this work is a specific regular black hole with an asymptotically Minkowski core, as discussed in [62,63]. This is an example of a metric with an exponential mass suppression, and is described by the line element

$$ds^2 = -\left(1 - \frac{2m e^{-a/r}}{r}\right) dt^2 + \frac{dr^2}{1 - \frac{2m e^{-a/r}}{r}} + r^2(d\theta^2 + \sin^2\theta d\phi^2). \tag{2}$$

A rather different (extremal) version of this model spacetime, based on nonlinear electrodynamics, was previously discussed by Culetu [64], with follow-up on some aspects of the non-extremal case in [65–67] (see also [68,69]).

Most regular black holes have a core that is asymptotically de Sitter (with constant positive curvature) [19–22]. However, the regular black hole described by the metric (2) has an asymptotically Minkowski core (in the sense that the stress-energy tensor asymptotes to zero). Such models have some attractive features compared to the more common de Sitter core regular black holes: the stress–energy tensor vanishes at the core, greatly simplifying the physics in this region; and many messy algebraic expressions are replaced by simpler expressions involving the exponential and Lambert  $W$  functions, whilst still allowing for explicit closed form expressions for quantities of physical interest [62]. Additionally, the results obtained in this work reproduce the standard results for the Schwarzschild metric by letting the parameter  $a \rightarrow 0$ . Thus, the value of the parameter  $a$  determines the extent of the “deviation” from the Schwarzschild spacetime.

If  $0 < a < 2m/e$ , then the spacetime described by the metric (2) has two horizons located at

$$r_{H^-} = 2m e^{W_{-1}(-\frac{a}{2m})}, \quad \text{and} \quad r_{H^+} = 2m e^{W_0(-\frac{a}{2m})}. \tag{3}$$

Here,  $W_{-1}(x)$  and  $W_0(x)$  are the real-valued branches of Lambert  $W$  function. We could also write

$$r_{H^-} = \frac{a}{|W_{-1}(-\frac{a}{2m})|}, \quad \text{and} \quad r_{H^+} = \frac{a}{|W_0(-\frac{a}{2m})|}. \tag{4}$$

Perturbatively, for small  $a$ , we have

$$r_{H^+} = 2m - a + \mathcal{O}(a^2), \tag{5}$$

nicely reproducing Schwarzschild in the  $a \rightarrow 0$  limit. For the inner horizon, since  $r_{H^-} < 2m$ ,

$$r_{H^-} = \frac{a}{\ln(2m/r_{H^-})} \tag{6}$$

implies  $r_{H^-} < a$ , whence we have a strict upper bound given by the simple analytic expression:

$$r_{H^-} < \frac{a}{\ln(2m/a)}. \tag{7}$$

Certainly,  $\lim_{a \rightarrow 0} r_{H^-}(m, a) = 0$  as we would expect to recover Schwarzschild; however, the form of  $r_{H^-}(m, a)$  is not analytic. This bound can also be viewed as the first term in an asymptotic expansion [70] based on (as  $x \rightarrow 0^+$ )

$$W_{-1}(-x) = \ln(x) + \mathcal{O}(\ln(-\ln(x))) = -\ln(1/x) + \mathcal{O}(\ln(\ln(1/x))). \tag{8}$$

This leads to

$$r_{H^-} = \frac{a}{\ln(2m/a) + \mathcal{O}(\ln(\ln(2m/a)))} = \frac{a}{\ln(2m/a)} + \mathcal{O}\left(\frac{a \ln(\ln(2m/a))}{(\ln(2m/a))^2}\right). \tag{9}$$

More specifically (as  $a/m \rightarrow 0$  or  $m/a \rightarrow \infty$ ),

$$\frac{r_{H^-}}{a} = \frac{1}{\ln(2m/a)} + \mathcal{O}\left(\frac{\ln(\ln(2m/a))}{(\ln(2m/a))^2}\right). \tag{10}$$

If  $a = 2m/e$ , then the two horizons merge at  $r_H = 2m/e = a$  and one has an extremal black hole. If  $a > 2m/e$ , then there are no horizons, and one is dealing with a regular horizonless extended but compact object (the energy density peaks at  $r = a/4$ ).

This object could either be extended all the way down to  $r = 0$ , or alternatively be truncated at some finite value of  $r$ , to be used as the exterior geometry for some static and spherically symmetric mass source that *is not* a black hole. This is potentially useful as a model for planets, stars, etc. Consequently, we also incorporate aspects of the analysis for  $a > 2m/e$  as and when required to generate astrophysical observables in the case when Equation (2) is modeling a compact object other than a black hole.

### 2. Geodesics and the Effective Potential

Continuing the analysis of [62], we now calculate the location of the photon sphere and extremal stable circular orbit (ESCO) for the regular black hole with line element given by equation (2). Photon spheres (or more precisely the closely related Sgr black hole silhouettes) have been recently observed for the massive objects M87 and Sgr A\* [53–58]. As such, they are, along with the closely related ESCOs, practical and useful quantities to calculate for black hole mimickers.

We begin by considering the affinely parameterized tangent vector to the worldline of a massive or massless particle in our spacetime (2):

$$g_{\mu\nu} \frac{dx^\mu}{d\lambda} \frac{dx^\nu}{d\lambda} = -\left(1 - \frac{2m e^{-a/r}}{r}\right) \left(\frac{dt}{d\lambda}\right)^2 + \left(\frac{1}{1 - \frac{2m e^{-a/r}}{r}}\right) \left(\frac{dr}{d\lambda}\right)^2 + r^2 \left[\left(\frac{d\theta}{d\lambda}\right)^2 + \sin^2 \theta \left(\frac{d\phi}{d\lambda}\right)^2\right] = \epsilon, \tag{11}$$

where  $\epsilon \in \{-1, 0\}$ , with  $-1$  corresponding to a massive (timelike) particle and  $0$  corresponding to a massless (null) particle. (The case  $\epsilon = +1$  would correspond to tachyonic particles following spacelike geodesics, a situation of no known physical applicability.) Since we are working with a spherically symmetric spacetime, we can set  $\theta = \pi/2$  without any loss of generality and reduce Equation (11) to

$$g_{\mu\nu} \frac{dx^\mu}{d\lambda} \frac{dx^\nu}{d\lambda} = -\left(1 - \frac{2m e^{-a/r}}{r}\right) \left(\frac{dt}{d\lambda}\right)^2 + \left(\frac{1}{1 - \frac{2m e^{-a/r}}{r}}\right) \left(\frac{dr}{d\lambda}\right)^2 + r^2 \left(\frac{d\phi}{d\lambda}\right)^2 = \epsilon. \tag{12}$$

Due to the presence of time-translation and angular Killing vectors, we can now define the conserved quantities

$$E = \left(1 - \frac{2m e^{-a/r}}{r}\right) \left(\frac{dt}{d\lambda}\right) \quad \text{and} \quad L = r^2 \left(\frac{d\phi}{d\lambda}\right), \tag{13}$$

corresponding to the energy and angular momentum of the particle, respectively. Thus, Equation (12) implies

$$E^2 = \left(\frac{dr}{d\lambda}\right)^2 + \left(1 - \frac{2m e^{-a/r}}{r}\right) \left(\frac{L^2}{r^2} - \epsilon\right). \tag{14}$$

This defines an “effective potential” for geodesic orbits

$$V_\epsilon(r) = \left(1 - \frac{2m e^{-a/r}}{r}\right) \left(\frac{L^2}{r^2} - \epsilon\right), \tag{15}$$

with the circular orbits corresponding to extrema of this potential.

### 3. Photon Spheres

We subdivide the discussion into two topics: First the *existence* of circular photon orbits (photon spheres) and then the *stability* of circular photon orbits. The discussion is considerably more complex than for the Schwarzschild spacetime, where there is only one circular photon orbit, at  $r = 3m$ , and that circular photon orbit is unstable. Once the extra parameter  $a$  is nonzero, and in particular sufficiently large, the set of photon orbits exhibits more diversity.

#### 3.1. Existence of Photon Spheres

For null trajectories, we have

$$V_0(r) = \left(1 - \frac{2m e^{-a/r}}{r}\right) \frac{L^2}{r^2}. \tag{16}$$

Thus, for circular photon orbits,

$$V'_0(r_c) = \frac{2L^2}{r_c^5} \left[ m e^{-a/r_c} (3r_c - a) - r_c^2 \right] = 0. \tag{17}$$

To be explicit about this, the location of a circular photon orbit,  $r_c$ , is given implicitly by the equation

$$r_c^2 = m e^{-a/r_c} (3r_c - a), \tag{18}$$

where  $a$  and  $m$  are fixed by the geometry of the spacetime.<sup>1</sup> The curve described by the loci of these circular photon orbits is plotted in two distinct ways in Figure 1.

For clarity, defining  $w = r_c/a$  and  $z = m/a$ , we can re-write the condition for circular photon orbits as

$$w^2 = z e^{-1/w} (3w - 1); \quad \implies \quad z = \frac{w^2 e^{1/w}}{3w - 1}. \tag{19}$$

In Figure 1, we also plot the locations of both inner and outer horizons.

The inner and outer horizons merge at  $a/m = 2/e = 0.7357588824\dots$ , i.e., at  $m/a = e/2 = 1.359140914\dots$ . For  $a/m > 2/e$ , i.e., for  $m/a < e/2$ , one is dealing with a horizonless compact object and we see that there is a region where there are *two* circular photon orbits. Note that the curve described by the loci of circular photon orbits terminates once one hits a horizon, i.e., at  $w = 1$ . Sub-horizon curves of constant  $r$  are spacelike (tachyonic), and *cannot* be lightlike, so they are explicitly excluded. That is, photon spheres can only *exist* in the region  $w \in (1, \infty)$ .

<sup>1</sup> As  $a \rightarrow 0$ , we have  $r_c \rightarrow 3m$ , as expected for Schwarzschild spacetime.

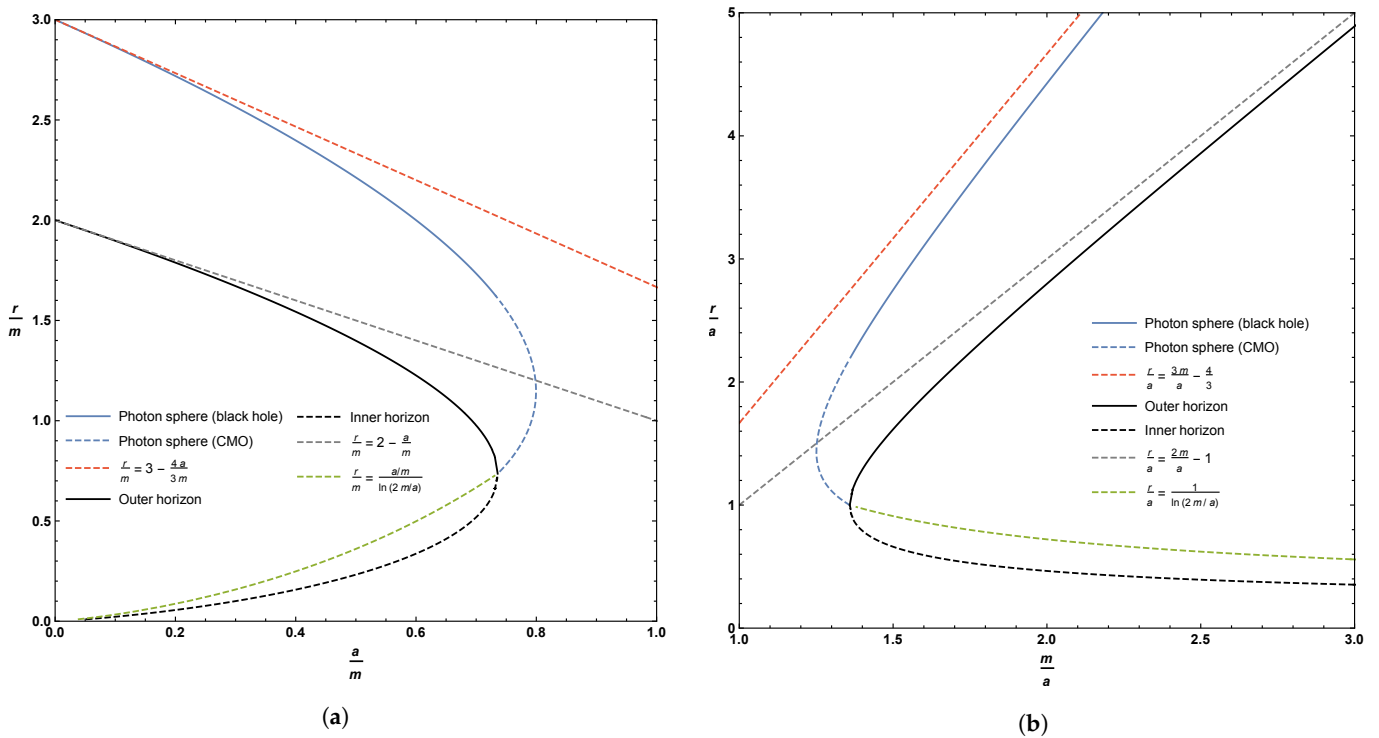


**Figure 1.** Location of the photon sphere, inner horizon, and outer horizon. Sub-figure (a) plots these quantities as a function of the parameter  $a$ ; sub-figure (b) plots these quantities as a function of the parameter  $m$ . The dashed blue line represents the extension of the photon sphere to horizonless compact massive objects (CMOs), whilst the dashed red line is the asymptotic solution for small values of the parameter  $a$  (Equation (21)). The dashed grey line is the asymptotic solution to the outer horizon for small values of  $a$  (Equation (5)). The dashed green line is the simple analytic bound and asymptotic estimate for the location of the inner horizon (Equations (7) and (10)).

Can we be more explicit about the key qualitative and quantitative features of this plot? Specifically, let us now analyze stability versus instability and find the exact location of the various turning points.

### 3.2. Stability versus Instability for Circular Photon Orbits

To check the *stability* of these circular photon orbits, we now need to investigate

$$V_0''(r_c) = \frac{2L^2}{r_c^7} \left[ 3r_c^3 - m e^{-a/r_c} (6r_c - a)(2r_c - a) \right]. \quad (20)$$

#### 3.2.1. Perturbative Analysis (small $a$ )

We note that determining  $r_c(m, a)$  from Equation (18) is not analytically feasible, but  $r_c(m, a)$  can certainly be estimated perturbatively for small  $a$ . We have

$$r_c(m, a) = 3m - \frac{4ma}{r_c} + \mathcal{O}(a^2) \implies r_c(m, a) = 3m - \frac{4}{3}a + \mathcal{O}(a^2). \quad (21)$$

Thus, for small values of  $a$ , we recover the standard result for the location of the photon sphere in Schwarzschild spacetime.

Estimating  $V_0''(r_c)$  by now substituting the approximate location of the photon sphere as  $r_c(m, a) = 3m - 4a/3 + \mathcal{O}(a^2)$ , we find

$$V_0''(r_c(m, a)) = -\frac{2L^2}{81m^4} \left( 1 + \frac{4}{3} \frac{a}{m} + \mathcal{O}(a^2) \right). \quad (22)$$

This quantity is manifestly negative for small  $a$ . That is, (within the limits of the current small- $a$  approximation), photons are in an unstable orbit at the small- $a$  photon sphere.

### 3.2.2. Non-Perturbative Analysis

However, if we rephrase the problem, then we can make some much more explicit exact statements that are no longer perturbative in small  $a$ : Whereas determining  $r_c(m, a)$  is analytically infeasible, it should be noted that in contrast both  $a(m, r_c)$  and  $m(r_c, a)$  are easily determined analytically:

$$a(m, r_c) = r_c(3 - W(r_c e^3/m)); \quad m(r_c, a) = \frac{r_c^2 e^{a/r_c}}{(3r_c - a)}. \tag{23}$$

Consequently, at the peak we can write

$$V_0(r_c, m) = \frac{L^2}{r_c^2} \left( 1 - \frac{2}{W(r_c e^3/m)} \right); \quad V_0(r_c, a) = \frac{L^2}{r_c^2} \frac{r_c - a}{3r_c - a}. \tag{24}$$

Regarding stability, in the first case, substituting (23) (left) into (20), we have

$$V_0''(r_c, m) = -\frac{2L^2(W(r_c e^3/m)^2 - W(r_c e^3/m) - 3)}{r_c^4 W(r_c e^3/m)}. \tag{25}$$

Using properties of the Lambert  $W$  function, we quickly see that this is negative for  $r_c/m > \frac{1}{2}(1 + \sqrt{13}) e^{-5/2 + \sqrt{13}/2} = 1.146702958\dots$ , implying instability of the circular photon orbits in this region, (and stability outside this region).

That is, on the curve of circular photon orbits,  $V''(r_c) = 0$  at the point

$$(r_c/m, a/m)_* = (1.146702958\dots, 0.7995092385\dots). \tag{26}$$

In the second case, substituting (23) (right) into (20), we have

$$V_0''(r_c, a) = -\frac{2L^2}{r_c^5} \frac{3r_c^2 - 5ar_c + a^2}{3r_c - a}. \tag{27}$$

This will certainly be negative for  $r_c/a > (5 + \sqrt{13})/6 = 1.434258546\dots$ , implying instability of the circular photon orbits in this region, (and stability outside this region).

That is, on the curve of circular photon orbits,  $V''(r_c) = 0$  at the point

$$(r_c/a, m/a)_* = (1.434258546\dots, 1.250767286\dots). \tag{28}$$

Consequently, on the curve of circular photon orbits, we have *existence* and *stability* in the region  $w \in (1, 1.434258546\dots)$  and *existence* and *instability* in the region  $w \in (1.434258546\dots, \infty)$ . Precisely at the point  $w = 1.434258546\dots$ , the photon sphere exhibits neutral stability.

### 3.3. Turning Points

To evaluate the exact location of the turning points on the curve described by the loci of circular photon orbits, recall that using  $w = r_c/a$  and  $z = m/a$  we can write this curve as

$$w^2 = z e^{-1/w} (3w - 1) \quad \implies \quad z = \frac{w^2 e^{1/w}}{(3w - 1)}. \tag{29}$$

This allows us to calculate

$$\frac{dz}{dw} = e^{1/w} \frac{3w^2 - 5w + 1}{(3w - 1)^2}, \tag{30}$$

which has a zero located at  $w = (5 + \sqrt{13})/6$ , where we have already seen that  $V_0''(r_c, a) = V_0''(w) = 0$ .

At this point,  $z$  takes on its maximum value

$$z = e^{6/(5+\sqrt{13})} \frac{(5 + \sqrt{13})^2}{18(3 + \sqrt{13})} = e^{(5-\sqrt{13})/2} \frac{(2 + \sqrt{13})}{9}. \tag{31}$$

Consequently, no photon sphere can exist if

$$\frac{a}{m} > e^{-(5-\sqrt{13})/2} (\sqrt{13} - 2) = 0.7995092385...; \tag{32}$$

or equivalently

$$\frac{m}{a} < e^{(5-\sqrt{13})/2} \frac{(2 + \sqrt{13})}{9} = 1.250767286... \tag{33}$$

Note that this happens when

$$\frac{r_c}{m} > \frac{1}{2}(1 + \sqrt{13})e^{-(5-\sqrt{13})/2}; \quad \frac{r_c}{a} > \frac{5 + \sqrt{13}}{6}, \tag{34}$$

which is where, as shown above,  $V_0'''(r_c, m) = 0$ .

As can be seen, originally in Figure 1, and now in more detail in the zoomed-in plot in Figure 2, for horizonless compact massive objects, there is a region where there are two possible locations for the photon sphere for fixed values of  $m$  and  $a$ . Furthermore, when this happens, it is the upper branch that corresponds to an unstable photon orbit, while the lower branch is a stable photon orbit.

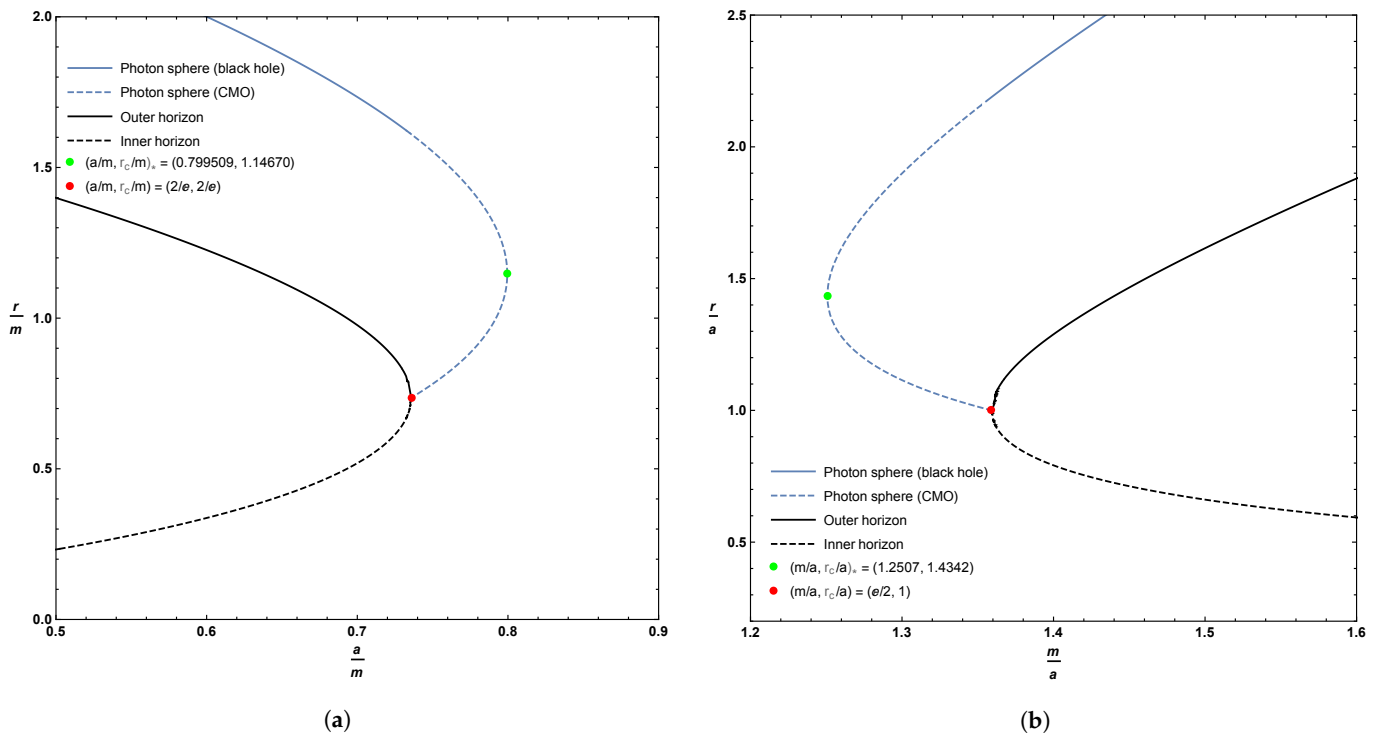


**Figure 2.** Zoomed in plots of the location of the photon sphere, inner horizon, and outer horizon, focusing on the extremal and merger regions. Sub-figure (a) plots these quantities as a function of the parameter  $a$ ; sub-figure (b) plots these quantities as a function of the parameter  $m$ . The dashed blue line represents the extension of the photon sphere to horizonless compact massive objects (CMOs). Whenever the location of the photon sphere is double-valued, the upper branch corresponds to an unstable photon orbit while the lower branch corresponds to a stable photon orbit.



#### 4. Timelike Circular Orbits

Let us first check the *existence*, and then the *stability*, of timelike circular orbits. Even in Schwarzschild spacetime ( $a \rightarrow 0$ ) this is not entirely trivial: Timelike circular orbits *exist* for all  $r_c \in (3m, \infty)$ ; they are unstable for  $r_c \in (3m, 6m)$ , exhibit neutral stability at  $r_c = 6m$ , and are stable for  $r_c \in (6m, \infty)$ . Once the parameter  $a$  is non-zero the situation is much more complex.

##### 4.1. Existence of Circular Timelike Orbits

For timelike trajectories, the effective potential is given by

$$V_{-1}(r) = \left(1 - \frac{2m e^{-a/r}}{r}\right) \left(1 + \frac{L^2}{r^2}\right), \tag{35}$$

and so the locations of the circular orbits can be found from

$$V'_{-1}(r_c) = -\frac{2}{r_c^5} \left\{ L^2 r_c^2 + m e^{-a/r_c} [a(L^2 + r_c^2) - r_c(3L^2 + r_c^2)] \right\} = 0. \tag{36}$$

That is, all timelike circular orbits (there will be infinitely many of them) must satisfy

$$L^2 r_c^2 + m e^{-a/r_c} [a(L^2 + r_c^2) - r_c(3L^2 + r_c^2)] = 0. \tag{37}$$

This is not analytically solvable for  $r_c(L, m, a)$ , however we *can* solve for the required angular momentum  $L_c(r_c, m, a)$  of these circular orbits:

$$L_c(r_c, m, a)^2 = \frac{r_c^2 m (r_c - a)}{ma - 3mr_c + r_c^2 e^{a/r_c}}. \tag{38}$$

Physically, we must demand  $0 \leq L_c^2 < \infty$ , so the boundaries for the *existence* region of circular orbits (whether stable or unstable) are given by

$$r_c = a; \quad ma - 3mr_c + r_c^2 e^{a/r_c} = 0. \tag{39}$$

The first of these conditions,  $r_c = a$ , comes from the fact that in this spacetime gravity is effectively repulsive for  $r < a$ . Remember that  $g_{tt} = -(1 - 2me^{-a/r}/r)$ , and that the pseudo-force due to gravity depends on  $\partial_r g_{tt}$ . Specifically,

$$\partial_r g_{tt} = -\frac{2m}{r^2} e^{-a/r} \left(1 - \frac{a}{r}\right), \tag{40}$$

and this changes sign at  $r = a$ . Thus, for  $r > a$ , gravity attracts you to the center, but for  $r < a$  gravity repels you from the center.

If gravity repels you, there is no way to counter-balance it with a centrifugal pseudo-force, and so there is simply no way to get a circular orbit, regardless of whether it is stable or unstable. Precisely at  $r = a$ , there are stable “orbits” where the test particle just sits there, with zero angular momentum, no sideways motion required. Since by construction  $r_c > r_{H^+} \geq a$ , this constraint is relevant only for horizonless CMOs.

The second of these conditions is exactly the location of the photon orbits considered in the previous sub-section. (Physically, what is going on is this: At large distances, it is easy to put a massive particle into a circular orbit with  $L_c \propto \sqrt{mr_c}$ . As one moves inwards and approaches the photon orbit, the massive particle must move more and more rapidly, and the angular momentum per unit mass must diverge when a particle with nonzero invariant mass tries to orbit at the photon orbit.)

Thus, the existence region (rather than just its boundary) for timelike circular orbits is (see Figure 3):

$$r_c > a; \quad ma - 3mr_c + r_c^2 e^{a/r_c} > 0 \tag{41}$$



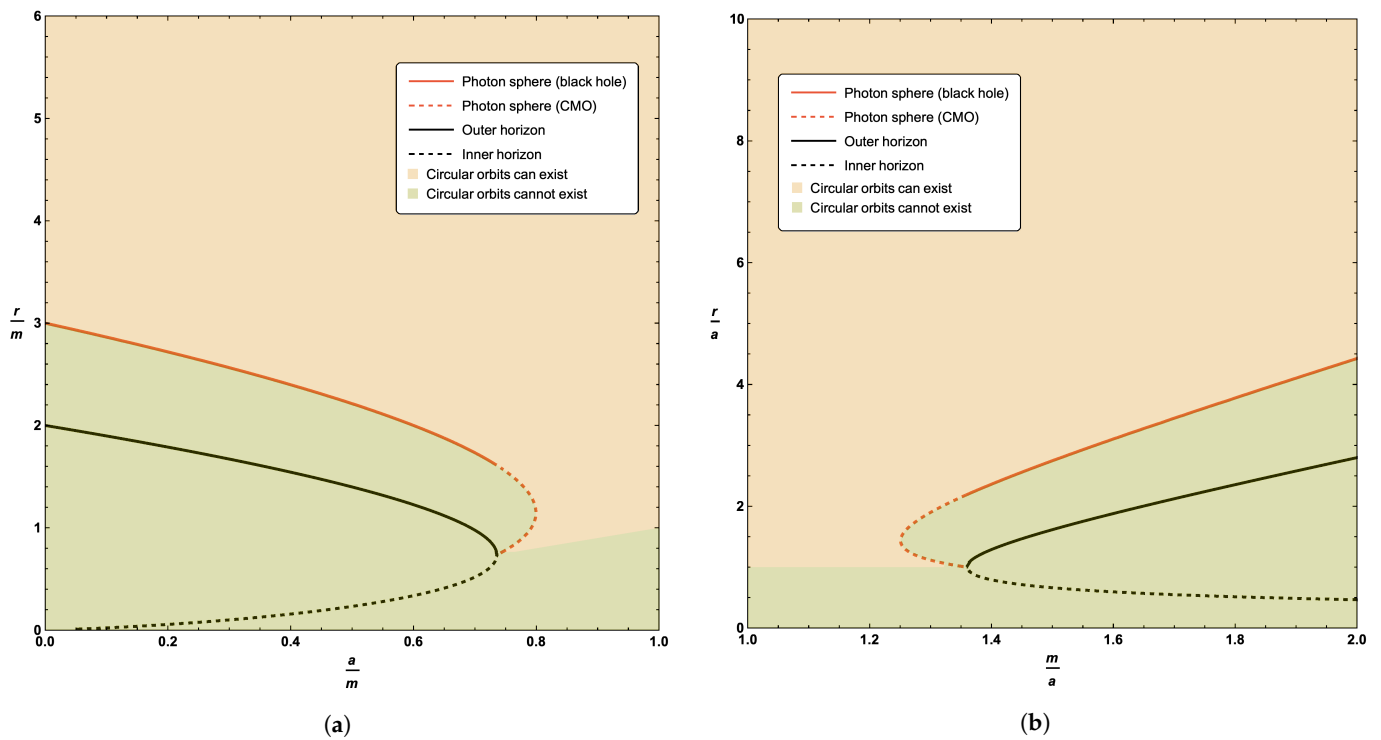


**Figure 3.** Locations of the *existence* region for timelike circular orbits in terms of the circular null geodesics, outer horizon, and inner horizon. Sub-figure (a) plots these quantities as a function of the parameter  $a$ ; sub-figure (b) plots these quantities as a function of the parameter  $m$ .

#### 4.2. Stability versus Instability for Circular Timelike Orbits

Now, consider the general expression

$$V''_{-1}(r) = \frac{6L^2r^3 - 2m(2r^4 - 4ar^3 + (12L^2 + a^2)r^2 - 8L^2ar + L^2a^2)e^{-a/r}}{r^7}, \tag{42}$$

and substitute the known value of  $L \rightarrow L_c(r_c)$  for circular orbits (see (38)). Then,

$$V''_{-1}(r_c) = -\frac{2me^{-a/r_c}(2m(3r_c^2 - 3ar_c + a^2)e^{-a/r_c} - r_c(r_c^2 + ar_c - a^2))}{(r_c^2 - m(3r_c - a)e^{-a/r_c})r^4}. \tag{43}$$

Note that  $V''_{-1}(r_c) \rightarrow \infty$  at the photon orbit (where the denominator has a zero).

To locate the *boundary* of the region of *stable* circular orbits, the ESCO (extremal stable circular orbit), we now need to set  $V''_{-1}(r_c) = 0$ , leading to the equation

$$2m(3r_c^2 - 3ar_c + a^2)e^{-a/r_c} = r_c(r_c^2 + ar_c - a^2). \tag{44}$$

We note that locating this boundary is equivalent to extremizing  $L_c(r_c)$ . To see this, consider the quantity  $[V'_{-1}(L(r), r)] = 0$  and differentiate:

$$\frac{d[V'_{-1}(L(r), r)]}{dr} = \left. \frac{\partial V'_{-1}(L, r)}{\partial L} \right|_{L=L(r)} \times \frac{dL(r)}{dr} + V''_{-1}(L, r)|_{L=L(r)}. \tag{45}$$

This implies

$$0 = \left. \frac{\partial V'_{-1}(L, r)}{\partial L} \right|_{L=L(r)} \times \frac{dL(r)}{dr} + V''_{-1}(L, r)|_{L=L(r)}. \tag{46}$$

Thence,

$$V''_{-1}(L, r)|_{L=L(r)} = - \left. \frac{\partial V'_{-1}(L, r)}{\partial L} \right|_{L=L(r)} \times \frac{dL(r)}{dr}. \quad (47)$$

However, it is easily checked that  $\partial V'_{-1}(L, r)/\partial L$  is non-zero outside the photon sphere (that is, in the existence region for circular timelike geodesics). Thence,

$$V''_{-1}(L, r)|_{L=L(r)} = 0 \quad \iff \quad \frac{dL(r)}{dr} = 0. \quad (48)$$

Thus, one might also extremize  $L_c^2(r_c)$ , as in Equation (38), and once again find Equation (44).

Defining  $w = r_c/a$  and  $z = m/a$ , the curve describing the boundary of the region of stable timelike circular orbits can be rewritten as

$$2z(3w^2 - 3w + 1)e^{-1/w} = w(w^2 + w - 1). \quad (49)$$

Plots of the boundary implied by Equation (44), or equivalently (49), can be seen in Figure 4. As for the photon sphere, we have the interesting result that the extension of the ESCO to horizonless compact massive objects results in up to two possible ESCO locations for fixed values of  $a$  and  $m$ . Perhaps unexpectedly, the curve of ESCOs does not terminate at the horizon—it terminates once it hits the curve of circular photon orbits at a very special point. Let us now turn to the detailed analysis of both the qualitative behavior and the various turning points presented in Figures 4 and 5. Note that where the ESCO is single-valued, it is an ISCO (innermost stable circular orbit). Where the ESCO is double-valued, the upper branch is an ISCO and the lower branch is an OSCO (outermost stable circular orbit) [71].

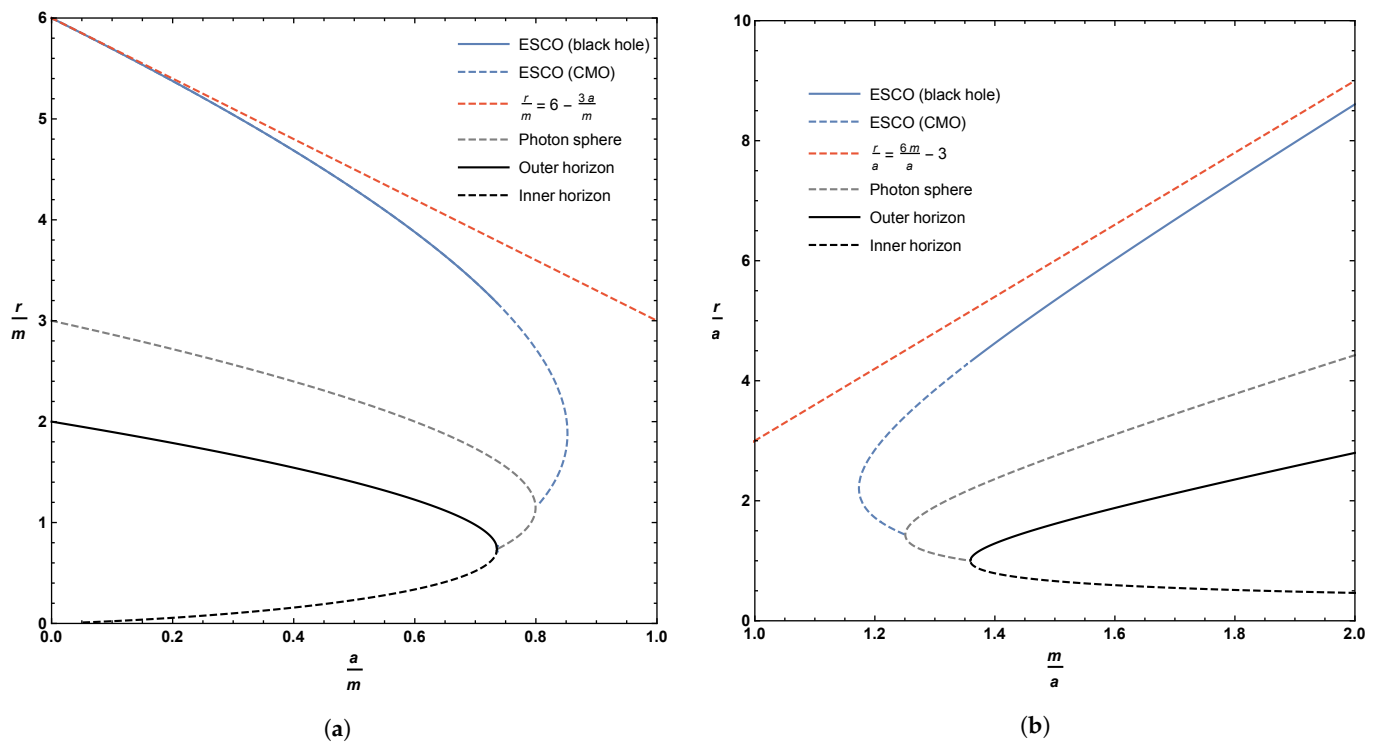


**Figure 4.** Locations of the ESCO, photon sphere, outer horizon, and inner horizon. Sub-figure (a) plots these quantities as a function of the parameter  $a$ ; sub-figure (b) plots these quantities as a function of the parameter  $m$ . The dashed blue line represents the extension of the ESCO to CMOs. The dashed red curves in (a,b) are the asymptotic location of the ISCO for small values of  $a$  (approaching the Schwarzschild solution).

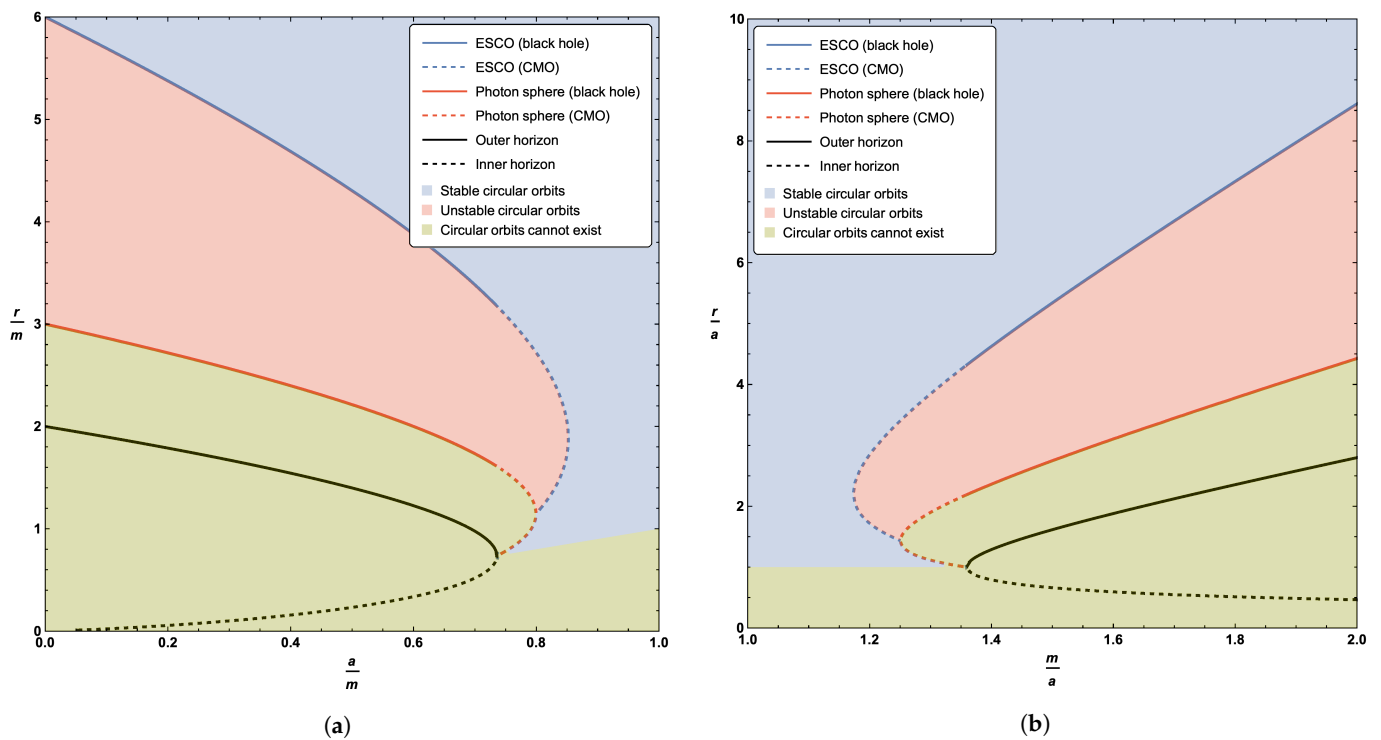


**Figure 5.** Locations of the ESCO, photon sphere, outer horizon, and inner horizon. Sub-figure (a) plots these quantities as a function of the parameter  $a$ ; sub-figure (b) plots these quantities as a function of the parameter  $m$ . The dashed blue line represents the extension of the ESCO to CMOs. The dashed red line represents the extension of the photon sphere to CMOs. The blue region denotes stable timelike circular orbits, while the red region denotes unstable timelike circular orbits, and the green region denotes the non-existence of timelike circular orbits. Where the ESCO is single-valued, it is an ISCO. Where the ESCO is double-valued, the upper branch is an ISCO and the lower branch is an OSCO (outermost stable circular orbit).

### 4.2.1. Perturbative Analysis (Small $a$ )

Let us first investigate the existence region perturbatively for small  $a$ . We have

$$L_c(r_c, m, a)^2 = \frac{mr_c^2}{r_c - 3m} - \frac{2mr_c(r_c - m)}{(r_c - 3m)^2} a + \mathcal{O}(a^2). \tag{50}$$

Note that this approximation diverges at the Schwarzschild photon sphere  $r = 3m$ . Thus, for small  $a$  the boundary for the region of *existence* of timelike circular orbits is still  $r = 3m$ .

Now, we investigate the *stability* region perturbatively for small  $a$ . Rearranging Equation (44), we see

$$r_c = \frac{6m(r_c^2 - ar_c + a^2/3)e^{-a/r_c}}{r_c^2 + ar_c - a^2} = 6m \left( 1 - \frac{3a}{r_c} + \mathcal{O}(a^2) \right). \tag{51}$$

Thence,

$$r_c = 6m - 3a + \mathcal{O}(a^2), \tag{52}$$

which sensibly reproduces the Schwarzschild ISCO to lowest order in  $a$ , and explains the asymptote in Figure 4b.

Furthermore, for small  $a$ , substituting  $L_c(r_c)$  into  $V''_{-1}(L, r_c)$  and expanding

$$V''_{-1}(r_c) = \frac{2m(r_c - 6m)}{r_c^3(r_c - 3m)} + \frac{4m^2(7r_c - 15m)}{r_c^4(r_c - 3m)^2} a + \mathcal{O}(a^2) \tag{53}$$

Demanding that this quantity be zero self-consistently yields  $r_c = 6m - 3a + \mathcal{O}(a^2)$ .

### 4.2.2. Non-Perturbative Analysis

We show above that, defining  $w = r_c/a$  and  $z = m/a$ , the curve describing the boundary of the region of stable timelike circular orbits can be rewritten as

$$2z(3w^2 - 3w + 1)e^{-1/w} = w(w^2 + w - 1). \tag{54}$$

Thence,

$$z = \frac{w(w^2 + w - 1)e^{1/w}}{2(3w^2 - 3w + 1)}. \tag{55}$$

Let us look for the turning points of  $z(w)$ . The derivative is

$$\frac{dz}{dw} = \frac{(w - 1)(3w^4 - 6w^3 - 3w^2 + 4w - 1)e^{1/w}}{2w(3w^2 - 3w + 1)^2}. \tag{56}$$

There is one obvious local extrema at  $w = 1$ , corresponding to  $z = e/2$ . Physically, this corresponds to the point where inner and outer horizon merge and become extremal—but from inspection of Figure 4, the descriptive plots of Figure 5, and the zoomed-in plots of Figure 6, we see that the curve of ESCOs hits the photon orbit (and becomes unphysical) before getting to this point. In terms of the variables used when plotting Figures 4–6, this unphysical (from the point of view of ESCOs) point corresponds to

$$(r_c/a, m/a)_* = (1, e/2) \quad (r_c/m, a/m)_* = (2/e, 2/e). \tag{57}$$

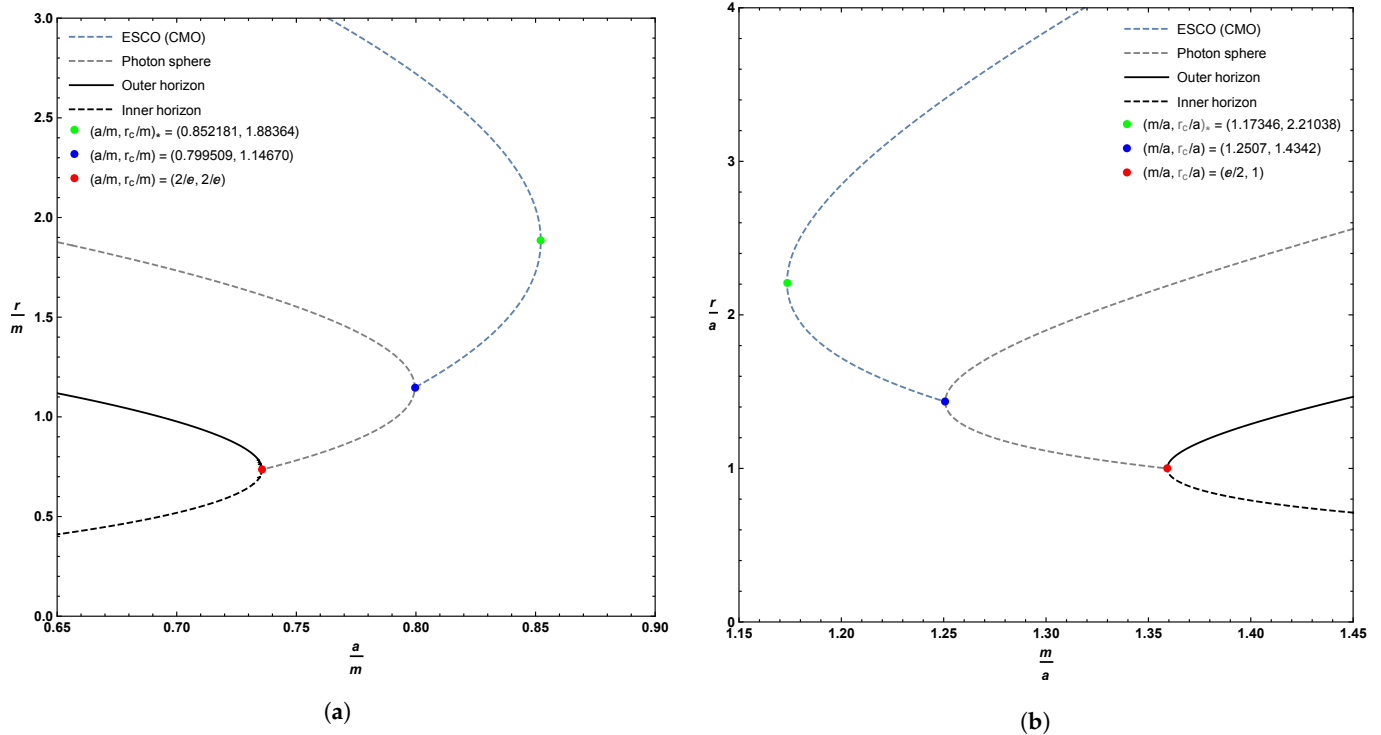


**Figure 6.** Zoomed in plot of the locations of the ESCO, outer horizon, and inner horizon for various values of the parameters  $a$  and  $m$ , focusing on the turning points. Sub-figure (a) plots these quantities as a function of the parameter  $a$ ; sub-figure (b) plots these quantities as a function of the parameter  $m$ . The dashed blue line represents the extension of the ESCO to CMOs. Where the ESCO is single-valued, it is an ISCO. Where the ESCO is double-valued, the upper branch is an ISCO and the lower branch is an OSCO.

The other local extrema is located at the only physical root of the quartic polynomial

$$3w^4 - 6w^3 - 3w^2 + 4w - 1 = 0. \tag{58}$$

While this can be solved analytically, the results are too messy to be enlightening and so we resort to numerics. Two roots are complex, one is negative, and the only physical root is  $w = 2.210375896\dots$ , corresponding to  $z = 1.173459017\dots$ . Physically, this implies that the ESCO curve should exhibit a non-trivial local extremum—and from inspection of Figure 4 we see that the curve of ESCOs does indeed have a local extremum at this point. In terms of the variables used when plotting Figure 4, this extremal point corresponds to

$$(r_c/a, m/a)_* = (2.210375896, 1.173459017), \tag{59}$$

and

$$(r_c/m, a/m)_* = (1.883641323, 0.8521814444). \tag{60}$$

### 4.3. Intersection of ESCO and Photon Sphere

We can rewrite the curve for the loci of the photon spheres (19) as

$$e^{-1/w} z = \frac{w^2}{(3w - 1)}. \tag{61}$$

Similarly, for the loci of ESCOs, we rewrite (55) as

$$e^{-1/w} z = \frac{w(w^2 + w - 1)}{2(3w^2 - 3w + 1)}. \tag{62}$$

These curves cross at

$$\frac{w}{(3w - 1)} = \frac{(w^2 + w - 1)}{2(3w^2 - 3w + 1)}. \tag{63}$$

That is, at

$$(w - 1)(3w^2 - 5w + 1) = 0, \tag{64}$$

with explicit roots at

$$1, \frac{5 \pm \sqrt{13}}{6}. \tag{65}$$

The physically relevant root is  $w = \frac{5+\sqrt{13}}{6} = 1.434258546\dots$ , which is where we determine above that the photon sphere became stable and at the point where the curve of photon spheres maximizes the value of  $z = m/a$ .

#### 4.4. Explicit Result for the Angular Momentum

We can rewrite the curve for the angular momentum (38) as

$$L_c^2 = a^2 \left( \frac{e^{-1/w_z} w^2 (w - 1)}{w^2 - e^{-1/w_z} (3w - 1)} \right). \tag{66}$$

Similarly, for the loci of ESCOs, we can rewrite (55) as

$$e^{-1/w_z} = \frac{w(w^2 + w - 1)}{2(3w^2 - 3w + 1)}. \tag{67}$$

We then substitute this into back into  $L_c$ :

$$L_c^2 = a^2 \frac{w^2(w^2 + w - 1)}{3w^2 - 5w + 1}. \tag{68}$$

This has a pole at  $w = \frac{5+\sqrt{13}}{6} = 1.434258546\dots$ , and is then positive and finite for all  $w > \frac{5+\sqrt{13}}{6}$ . (Of course, the point  $w = \frac{5+\sqrt{13}}{6}$  on the ESCO curve is exactly where the ESCO curve hits the photon curve, so we would expect the angular momentum to go to infinity there.) Asymptotically, for large  $r$  (large  $w = r_c/a$ ), we have  $L_c^2 \sim a^2 w^2/3$  and  $m/a = z \sim w/6$ , so  $L_c^2 \sim 2mr_c$  as expected from the large-distance Newtonian limit.

#### 4.5. Summary

Overall, we see that the boundary of the stability region for timelike circular orbits is rather complicated. In terms of the variable  $w = r_c/a$ :

- For  $w \in (\frac{5+\sqrt{13}}{6}, \infty)$ , we have an ESCO. This ESCO then subdivides as follows:
  - For  $w \in (2.210375896, \infty)$ , we have an ISCO.
  - For  $w \in (\frac{5+\sqrt{13}}{6}, 2.210375896)$ , we have an OSCO.
- For  $w \in (1, \frac{5+\sqrt{13}}{6})$ , the stability region is bounded by a stable photon orbit.
- The line  $w = 1$  bounds the stability and existence region for timelike circular orbits from below.

This is considerably more complicated than might reasonably have been expected.

### 5. Conclusions

In this work, we investigate astrophysically observable quantities of a specific novel regular black hole model based on an asymptotically Minkowski core [62,63]: Specifically, we investigate the photon sphere and ESCO. The spacetime under consideration is an example of a black hole mimicker. For the regular black hole model, both the photon

sphere and the ESCO exist and are located outside of the outer horizon, and thus (at least in theory) could be astrophysically observable. The analysis of the photon sphere and ESCO is extended to horizonless compact massive objects, leading to the surprising results that, for fixed values of  $m$  and  $a$ , up to two possible photon sphere and up to two possible ESCO locations exist in our model spacetime; and that the very existence of the photon sphere and ESCO depends explicitly on the ratio  $a/m$ . Somewhat unexpectedly, due to the effectively repulsive nature of gravity in the region near the core, we find some situations in which the photon orbits are stable and some situations where the ESCOs are OSCOs rather than ISCOs. There is a rich phenomenology here that is significantly more complex than for the Schwarzschild spacetime.

**Author Contributions:** Conceptualization, T.B., A.S. and M.V.; methodology, T.B., A.S. and M.V.; software, T.B., A.S. and M.V.; validation, T.B., A.S. and M.V.; formal analysis, T.B., A.S. and M.V.; resources, M.V.; writing—original draft preparation, T.B., A.S. and M.V.; writing—review and editing, T.B., A.S. and M.V.; visualization, T.B., A.S. and M.V.; supervision, M.V.; project administration, M.V.; and funding acquisition, M.V. All authors have read and agreed to the published version of the manuscript.

**Funding:** TB was supported by a Victoria University of Wellington MSc scholarship and was also indirectly supported by the Marsden Fund, via a grant administered by the Royal Society of New Zealand. AS acknowledges financial support via a PhD Doctoral Scholarship provided by Victoria University of Wellington. AS is also indirectly supported by the Marsden fund, via a grant administered by the Royal Society of New Zealand. MV was directly supported by the Marsden Fund, via a grant administered by the Royal Society of New Zealand.

**Conflicts of Interest:** The authors declare no conflict of interest.

## Abbreviations

The following abbreviations are used in this manuscript:

ESCO	Extremal stable circular orbit
ISCO	Innermost stable circular orbit
OSCO	Outermost stable circular orbit
CMO	Compact massive object

## References

- Schwarzschild, K. Über das Gravitationsfeld eines Massenpunktes nach der Einsteinschen Theorie. *Sitzungsberichte Der Königlich Preuss. Akad. Der Wiss.* **1916**, *7*, 189.
- Reissner, H. Über die Eigengravitation des elektrischen Feldes nach der Einsteinschen Theorie. *Ann. Der Phys.* **1916**, *50*, 106. [[CrossRef](#)]
- Weyl, H. Zur Gravitationstheorie. *Ann. Der Phys.* **1917**, *54*, 117. [[CrossRef](#)]
- Nordström, G. On the Energy of the Gravitational Field in Einstein's Theory. *Verhandl. Koninkl. Ned. Akad. Wetenschap. Afdel. Natuurk.* **1918**, *24*, 1201.
- Kerr, R. Gravitational Field of a Spinning Mass as an Example of Algebraically Special Metrics. *Phys. Rev. Lett.* **1963**, *11*, 237. [[CrossRef](#)]
- Newmann, E.; Couch, E.; Chinnapared, K.; Exton, A.; Prakash, A.; Torrence, R. Metric of a Rotating, Charged Mass. *J. Math. Phys.* **1965**, *6*, 918. [[CrossRef](#)]
- Kerr, R.; Schild, A. Republication of: A new class of vacuum solutions of the Einstein field equations. *Gen. Rel. Grav.* **2009**, *41*, 2485. [[CrossRef](#)]
- Visser, M. The Kerr spacetime: A brief introduction. *arXiv* **2007**, arXiv:0706.0622.
- Wiltshire, D.L.; Visser, M.; Scott, S.M. *The Kerr Spacetime: Rotating Black Holes in General Relativity*; Cambridge University Press: Cambridge, UK, 2009.
- Baines, J.; Berry, T.; Simpson, A.; Visser, M. Unit-lapse versions of the Kerr spacetime. *arXiv* **2008**, arXiv:2008.03817
- Baines, J.; Berry, T.; Simpson, A.; Visser, M. Painleve–Gullstrand form of the Lense–Thirring spacetime. *arXiv* **2006**, arXiv:2006.14258
- Vaidya, P.C. The External Field of a Radiating Star in General Relativity. *Curr. Sci. (India)* **1943**, *12*, 183. [[CrossRef](#)]
- Vaidya, P.C. The external field of a radiating star. *Proc. Indian Acad. Sci.* **1951**, *33*, 264. [[CrossRef](#)]
- Vaidya, P.C. Nonstatic solutions of Einstein's field equations for spheres of fluids radiating energy. *Phys. Rev.* **1951**, *83*, 10. [[CrossRef](#)]
- Calmet, X. *Quantum Aspects of Black Holes*; Springer Int. Pub.: Heidelberg, Germany, 2015.



16. Calmet, X.; El-Menoufi, B.K. Quantum corrections to Schwarzschild black hole. *Eur. Phys. J. C* **2017**, *77*, 243. [[CrossRef](#)]
17. Kazakov, D.I.; Solodukhin, S.N. On quantum deformation of the Schwarzschild solution. *Nucl. Phys. B* **1994**, *429*, 153. [[CrossRef](#)]
18. Ali, A.F.; Khalil, M.M. Black hole with quantum potential. *Nucl. Phys. B* **2016**, *909*, 173. [[CrossRef](#)]
19. Bardeen, J.M. Non-singular general-relativistic gravitational collapse. In Proceedings of the International Conference GR5, Tbilisi, Georgia, USSR, 9–13 September 1968.
20. Hayward, S.A. Formation and Evaporation of Nonsingular Black Holes. *Phys. Rev. Lett.* **2006**, *96*, 031103. [[CrossRef](#)]
21. Frolov, V.P. Information loss problem and a ‘black hole’ model with a closed apparent horizon. *J. High Energy Phys.* **2014**, *2014*, 49. [[CrossRef](#)]
22. Ansoldi, S. Spherical black holes with regular center: A review of existing models including a recent realization with Gaussian sources. *arXiv* **2008**, arXiv:0802.0330.
23. Carballo-Rubio, R.; di Filippo, F.; Liberati, S.; Pacilio, C.; Visser, M. On the viability of regular black holes. *J. High Energy Phys.* **2018**, *2018*, 20. [[CrossRef](#)]
24. Morris, M.; Thorne, K.S. Wormholes in spacetime and their use for interstellar travel: A tool for teaching General Relativity. *Am. J. Phys.* **1988**, *56*, 395. [[CrossRef](#)]
25. Morris, M.S.; Thorne, K.S.; Yurtsever, U. Wormholes, Time Machines, and the Weak Energy Condition? *Phys. Rev. Lett.* **1988**, *61*, 1446. [[CrossRef](#)] [[PubMed](#)]
26. Visser, M. *Lorentzian Wormholes: From Einstein to Hawking*; Springer: New York, NY, USA, 1995.
27. Visser, M. Traversable wormholes: Some simple examples. *Phys. Rev. D* **1989**, *39*, 3182. [[CrossRef](#)] [[PubMed](#)]
28. Visser, M. Traversable wormholes from surgically modified Schwarzschild space-times. *Nucl. Phys. B* **1989**, *328*, 203–212, doi:10.1016/0550-3213(89)90100-4. [[CrossRef](#)]
29. Visser, M. Wormholes, Baby Universes and Causality. *Phys. Rev. D* **1990**, *41*, 1116. [[CrossRef](#)]
30. Visser, M.; Kar, S.; Dadhich, N. Traversable wormholes with arbitrarily small energy condition violations. *Phys. Rev. Lett.* **2003**, *90*, 201102. [[CrossRef](#)]
31. Visser, M. From wormhole to time machine: Comments on Hawking’s chronology protection conjecture. *Phys. Rev. D* **1993**, *47*, 554–565. [[CrossRef](#)]
32. Kar, S.; Dadhich, N.; Visser, M. Quantifying energy condition violations in traversable wormholes. *Pramana* **2004**, *63*, 859–864. [[CrossRef](#)]
33. Poisson, E.; Visser, M. Thin shell wormholes: Linearization stability. *Phys. Rev. D* **1995**, *52*, 7318–7321. [[CrossRef](#)]
34. Cramer, J.G.; Forward, R.L.; Morris, M.S.; Visser, M.; Benford, G.; Landis, G.A. Natural wormholes as gravitational lenses. *Phys. Rev. D* **1995**, *51*, 3117–3120. [[CrossRef](#)]
35. Dadhich, N.; Kar, S.; Mukherji, S.; Visser, M.  $R = 0$  space-times and selfdual Lorentzian wormholes. *Phys. Rev. D* **2002**, *65*, 064004. [[CrossRef](#)]
36. Boonserm, P.; Ngampitipan, T.; Simpson, A.; Visser, A. The exponential metric represents a traversable wormhole. *Phys. Rev. D* **2018**, *98*, 084048. [[CrossRef](#)]
37. Simpson, A.; Visser, M. Black-bounce to traversable wormhole. *JCAP* **2019**, *1902*, 42. [[CrossRef](#)]
38. Simpson, A.; Martín-Moruno, P.; Visser, M. Vaidya spacetimes, black-bounces, and traversable wormholes. *Class. Quant. Grav.* **2019**, *36*, 145007. [[CrossRef](#)]
39. Lobo, F.S.N.; Simpson, A.; Visser, M. Dynamic thin-shell black-bounce traversable wormholes. *Phys. Rev. D* **2020**, *101*, 124035. [[CrossRef](#)]
40. Mazur, P.O.; Mottola, E. Gravitational vacuum condensate stars. *Proc. Natl. Acad. Sci. USA* **2004**, *101*, 9545. [[CrossRef](#)]
41. Mazur, P.O.; Mottola, E. Gravitational Condensate Stars: An Alternative to Black Holes. *arXiv* **2001**, arXiv:0109035.
42. Visser, M.; Wiltshire, D. Stable gravastars: An alternative to black holes?. *Class. Quant. Grav.* **2004**, *21*, 1135. [[CrossRef](#)]
43. Cattoën, C.; Faber, T.; Visser, M. Gravastars must have anisotropic pressures. *Class. Quant. Grav.* **2005**, *22*, 4189–4202. [[CrossRef](#)]
44. Lobo, F.S.N. Stable dark energy stars. *Class. Quant. Grav.* **2006**, *23*, 1525. [[CrossRef](#)]
45. Martín-Moruno, P.; Montelongo-García, N.; Lobo, F.S.N.; Visser, M. Generic thin-shell gravastars. *JCAP* **2012**, *3*, 34. [[CrossRef](#)]
46. Lobo, F.S.N.; Martín-Moruno, P.; Montelongo-García, N.; Visser, M. Novel stability approach of thin-shell gravastars. *arXiv* **2015**, arXiv:1512.07659.
47. Cunha, P.V.; Berti, E.; Herdeiro, C.A.R. Light-Ring Stability for Ultracompact Objects. *Phys. Rev. Lett.* **2017**, *119*, 251102. [[CrossRef](#)] [[PubMed](#)]
48. Cunha, P.V.; Herdeiro, C.A.R. Stationary black holes and light rings. *Phys. Rev. Lett.* **2020**, *124*, 181101. [[CrossRef](#)] [[PubMed](#)]
49. Carballo-Rubio, R.; di Filippo, F.; Liberati, S.; Visser, M. Opening the Pandora’s box at the core of black holes. *Class. Quant. Grav.* **2020**, *37*, 145005. [[CrossRef](#)]
50. Visser, M.; Barceló, C.; Liberati, S.; Sonogo, S. Small, dark, and heavy: But is it a black hole? *PoS BHGRS* **2008**, *17*. [[CrossRef](#)]
51. Visser, M. Physical observability of horizons. *Phys. Rev. D* **2014**, *90*, 127502. [[CrossRef](#)]
52. Carballo-Rubio, R.; di Filippo, F.; Liberati, S.; Visser, M. Phenomenological aspects of black holes beyond general relativity. *Phys. Rev. D* **2018**, *98*, 124009. [[CrossRef](#)]
53. The Event Horizon Telescope Collaboration. First M87 Event Horizon Telescope Results. I. The Shadow of the Supermassive Black Hole. *ApJL* **2019**, *875*, L1. [[CrossRef](#)]

54. The Event Horizon Telescope Collaboration. First M87 Event Horizon Telescope Results. II. Array and Instrumentation. *ApJL* **2019**, *875*, L2. [[CrossRef](#)]
55. The Event Horizon Telescope Collaboration. First M87 Event Horizon Telescope Results. III. Data Processing and Calibration. *ApJL* **2019**, *875*, L3. [[CrossRef](#)]
56. The Event Horizon Telescope Collaboration. First M87 Event Horizon Telescope Results. IV. Imaging the Central Supermassive Black Hole. *ApJL* **2019**, *875*, L4. [[CrossRef](#)]
57. The Event Horizon Telescope Collaboration. First M87 Event Horizon Telescope Results. V. Physical Origin of the Asymmetric Ring. *ApJL* **2019**, *875*, L5. [[CrossRef](#)]
58. The Event Horizon Telescope Collaboration. First M87 Event Horizon Telescope Results. VI. The Shadow and Mass of the Central Black Hole. *ApJL* **2019**, *875*, L6. [[CrossRef](#)]
59. Collection of Detection Papers from LIGO. Publications from the LIGO Scientific Collaboration and Virgo Collaboration. Available online: <https://www.ligo.caltech.edu/page/detection-companion-papers> (accessed on 20 December 2020).
60. Current Gravitational Wave Observations. Available online: [wikipedia.org/List\\_of\\_gravitational\\_wave\\_observations](https://wikipedia.org/List_of_gravitational_wave_observations) (accessed on 20 December 2020).
61. Barausse, E.; Berti, E.; Hertog, T.; Hughes, S.A.; Jetzer, P.; Pani, P.; Sotiriou, T.P.; Tamanini, N.; Witek, H.; Yagi, K.; et al. Prospects for Fundamental Physics with LISA. *Gen. Rel. Grav.* **2020**, *52*, 8. [[CrossRef](#)]
62. Simpson, A.; Visser, M. Regular black holes with asymptotically Minkowski cores. *Universe* **2020**, *6*, 8. [[CrossRef](#)]
63. Berry, T.; Lobo, F.S.; Simpson, A.; Visser, M. Simpson and M. Visser, Thin-shell traversable wormhole crafted from a regular black hole with asymptotically Minkowski core. *Phys. Rev. D* **2020**, *102*, 064054. [[CrossRef](#)]
64. Culetu, H. On a regular modified Schwarzschild spacetime. *arXiv* **2013**, arXiv:1305.5964
65. Culetu, H. On a regular charged black hole with a nonlinear electric source. *Int. J. Theor. Phys.* **2015**, *54*, 2855. [[CrossRef](#)]
66. Culetu, H. Nonsingular black hole with a nonlinear electric source. *Int. J. Mod. Phys. D* **2015**, *24*, 1542001. [[CrossRef](#)]
67. Culetu, H. Screening an extremal black hole with a thin shell of exotic matter. *Phys. Dark Univ.* **2016**, *14*, 1. [[CrossRef](#)]
68. Junior, E.L.B.; Rodrigues, M.E.; Houndjo, M.J.S. Regular black holes in  $f(T)$  Gravity through a nonlinear electrodynamics source. *JCAP* **2015**, *1510*, 60. [[CrossRef](#)]
69. Rodrigues, M.E.; Junior, E.L.B.; Marques, G.T.; Zanchin, V.T. Regular black holes in  $f(R)$  gravity coupled to nonlinear electrodynamics. *Phys. Rev. D* **2016**, *94*, 024062. [[CrossRef](#)]
70. Corless, R.M.; Gonnet, G.H.; Hare, D.E.G.; Jeffrey, D.J.; Knuth, D.E. On the Lambert  $W$  function. *Adv. Comput. Math.* **1996**, *5*, 329–359. [[CrossRef](#)]
71. Boonserm, P.; Ngampitipan, T.; Simpson, A.; Visser, M. Innermost and outermost stable circular orbits in the presence of a positive cosmological constant. *Phys. Rev. D* **2020**, *101*, 24050. [[CrossRef](#)]